



Danial, J. S. H., Shalaby, R., Cosentino, K., Mahmoud, M. M., Medhat, F., Klenerman, D. and Garcia Saez, A. J. (2021) DeepSense: deep learning-based detection of single molecules. *Bioinformatics*, 37(21), pp. 3998-4000.

(doi: [10.1093/bioinformatics/btab352](https://doi.org/10.1093/bioinformatics/btab352))

This is the Author Accepted Manuscript.

There may be differences between this version and the published version. You are advised to consult the publisher's version if you wish to cite from it.

<https://eprints.gla.ac.uk/259852/>

Deposited on: 17 December 2021

DeepSinse: deep learning based detection of single molecules

John S H Danial^{1*}, Raed Shalaby^{2*}, Katia Cosentino³, Marwa M Mahmoud⁴, Fady Medhat⁵, David Klenerman¹ and Ana J Garcia Saez²

¹ Yusuf Hamied Department of Chemistry, University of Cambridge, Cambridge, United Kingdom

² Institute of Genetics, University of Cologne, Cologne, Germany

³ Department of Biology, University of Osnabrück, Osnabrück, Germany

⁴ Department of Computer Science, University of Cambridge, Cambridge, United Kingdom

⁵ Department of Computer Science, University of York, York, United Kingdom

* These authors contributed equally

Correspondence to: John S H Danial (js2494@cam.ac.uk)

Abstract

Imaging single molecules has emerged as a powerful characterization tool in the biological sciences. The detection of these under various noise conditions requires the use of algorithms that are dependent on the end-user inputting several parameters, the choice of which can be challenging and subjective. In this work, we propose DeepSinse, an easily-trainable and useable deep neural network that can detect single molecules with little human input and across a wide range of signal-to-noise ratios. We validate the neural network on the detection of single bursts in simulated and experimental data and compare its performance with the best-in-class, domain-specific algorithms.

Main

The detection of single molecules is a fundamental step in the computational pipeline dedicated to processing single molecule microscopy data. Counting^{1,2}, distancing^{3,4}, localising⁵⁻⁹ and tracking¹⁰⁻¹² single molecules require different imaging conditions and instrumentation resulting in fluorescent bursts characterised by low-to-high signal-to-noise ratios. This poses a challenge to the detection of single molecules using a universal algorithm. Segmentation of these molecules has, thus far, relied on user-chosen kernel functions, such as lowered Gaussians, Difference-of-Gaussians (DoG) or multi-order wavelets, and subjective, non-universal related parameters¹³. All these inputs are not intuitive to the amateur user, would require careful tuning before changing the imaging conditions or modality and may fail to appropriately segment single molecules under various signal-to-noise ratios yielding unreliable performance.

Deep neural networks were recently used in calculating the background under noisy imaging conditions¹⁸, localizing single emitters at high spatial densities^{14,15} and accurately counting molecular stoichiometries by step-wise photobleaching¹⁹. In this work, we developed and used DeepSinse, a simple, multi-layer Convolutional Neural Network (CNN) architecture to enable fast detection of single molecules using as few parameters as possible. Our neural network is composed of a CNN, a dense layer and a SoftMax (classification) layer. The neural network (**figure 1a**) was first trained to classify simulated ground-truth datasets of noise and Gaussian bursts in pre-labelled Regions Of Interest (ROIs), then validated on different, unseen, datasets of pre-labelled ROIs. We then tested it on ground-truth generated ROIs (**figure 1b**). The neural network is finally deployed by feeding an image into a peak-finding algorithm based on identifying regional maxima. The peak-finding algorithm outputs hundreds of noise- and burst- containing ROIs which are then fed into the trained network for classification, thus, resulting in an annotated image (**figure 1c**).

To construct the training dataset, 100 particles (bursts) were randomly scattered across images which are 200 by 200 pixels in size. The standard deviation of each burst was sampled using a random number generator confined between 1 and 2 pixels to simulate small and large particles. Each burst was convoluted with a 2D Gaussian Kernel. The produced images in counts I_c was modified as follows:

$$I_e = I_c * QE + DC + RO$$

Where I_e is the image signal in electrons, QE is the quantum efficiency, DC is the dark current and RO is the read out noise. The quantum efficiency was set at 95%, dark current was set at 0.0002 electrons/second and read out noise was set to 1 electron. These values are typical of commercially available Electron-Multiplying Charge Coupled Detectors (EMCCDs). To simulate noise, I_e was modified as follows:

$$I_e = \text{gamma} \left(I_e, G - 1 + \frac{1}{I_e} \right) + O$$

Where G is the camera gain (corrected for conversion factor) and O is the camera bias offset. The gain was set to 58.8 and offset to 400. This noise model was chosen to best replicate the electron-multiplication feature in emCCDs¹⁶. Burst-containing, and pure-noise, images were simulated with the formers' peak burst intensities varying from 50 to 100 counts corresponding to signal-to-noise ratios from 24.85 to 45.81 and 100 images were simulated with pure noise. Pre-annotated ROIs were picked from each of these images, intensity scaled between 0 and 1 to ensure the user avoids subjective segmentation parameters such as the intensity threshold, shuffled and fed into the neural network for training. To optimize performance, the neural network was trained using different ROI radii (**figure 2a**) and number of ROIs (**figure 2b**). The lowest FNR (61.45%) and FPR (0.3%) were achieved at a ROI radius of 5 pixels and 10,000 training ROIs.

To study the performance of DeepSense at varying SNRs, we first simulated 100 burst-containing images with peak burst intensities varying from 1 to 100 counts corresponding to signal-to-noise ratios from 2.17 to 45.81. At the lowest simulated SNR of 2.17 (where the particles are visually undiscernible), the FNR is 91.1% and FPR is 0%. At the highest simulated SNR of 45.81, the FNR is 0% and FPR is 0.1% (**figure 2c** and **e**). We then tested the performance of DeepSense with experimentally-obtained images of fluorescent beads (see **supplementary information**). At the lowest acquired mean SNR of 2.88, the measured FNR is 76.5% and FPR is 0.01%, whilst at the highest acquired mean SNR of 4.5, the measured FNR is 13.76% and FPR is 1.25% (**figure 2d** and **f**). We compare these metrics with the best in-class, domain-specific algorithm used for the detection of single molecules which is based on image wavelet segmentation¹³. Wavelet analysis achieves a FNR of 75% and FPR of 2% at an SNR of 2.6. These figures are worse than those measured with DeepSense, namely, a FNR of 15.5% (5x improvement) and FPR of 0.5% (4x improvement) and show the prominence of DeepSense in detecting single molecules under extreme noise conditions and low SNRs reaching 2.17.

To ensure applicability on a real biological sample acquired at the single molecule level, we used an exemplary dataset of a U2OS cell expressing the GFP-tagged nucleoporin component (Nup96) of the nuclear pore complex labelled with Alexa647-tagged-Anti-GFP nanobody and imaged using dSTORM¹⁷ (see **Data availability**). Molecules detected in single molecule localization microscopy are subjected to strict filtering to ensure the localization precision is minimized (see **Supplementary information**). We assessed the performance of DeepSense and wavelet filtering by comparing the number of detected particles pre filtering (**figure 3a**) and the fraction of rejected particles post filtering (**figure 3b**) in 1000 frames. DeepSense outperformed wavelet filtering, detecting 31331 particles (8810 of which were filtered corresponding to 28%) compared to 45131 for wavelet filtering with a peak intensity threshold applied (32747 of which were filtered corresponding to 73%) and 837129 without a peak intensity threshold applied (32747 of which were filtered corresponding to 99%). We, subsequently, used DeepSense to classify all ROIs extracted from 90,000 of the dataset and processed them in a similar fashion to that reported in¹⁷ to produce a super-resolved image where the ring-like structure of the nucleoporin assembly organized into an oligomer of 8-mer configuration was clearly resolvable as per the original account (**figure 3c**).

There are two important factors characterizing the performance of DeepSense: accuracy and speed. In the above, we provided an extensive comparison of the accuracy achieved by DeepSense in detecting single molecules, even at extremely low SNRs across simulated and experimental data. Since the performance of DeepSense is dependent on the simulated data resembling the experimental data, we expect the performance to be further improved if the training data is extracted from experimentally obtained images. For this reason, we have included a ROI-picker which the end user can utilize in selecting ROIs from experimental data to train the neural network (see **Data availability**). In terms of speed, DeepSense can be trained using 10,000 ROIs on a mid-class Graphical Processing Unit (GPU) NVIDIA GeForce GTX 1650 for 12 seconds or an Intel Core i7-9750H CPU running at 2.60GHz for 11 seconds. DeepSense can be deployed using 1,000 frames which are 200 by 200 pixels in size in 40 seconds using the named GPU or 1 minute and 20 seconds on the named CPU. By comparison, Wavelet filtering with, and without, the application of a peak intensity threshold takes 9 minutes, and 10 seconds, respectively.

DeepSense presents a novel paradigm in the detection of single molecules. The versatility, high selectivity, dependence on modest resources and speed in training and testing of the proposed neural network, as discussed above, are strong warrants for its adoption in all single molecule microscopy data processing pipelines. Importantly, our simple network does not depend on the application of any subjective peak

intensity threshold and is capable of detecting single molecules under extreme noise conditions; therefore, pushing detection limits with current instrumentation to new heights. Our proposed network can be augmented with other, previously-developed neural networks to migrate to smart and fully-automated analysis pipelines for single molecule microscopy data. To facilitate this, we have built an easy-to-use Graphical User Interface (GUI) for generating simulated data, training the neural network and accessing the performance of the trained network (see **Code availability**). Furthermore, we made available a number of pre-trained networks at different camera gain values which can be integrated in any MATLAB© based code (see **Code availability**).

Data availability

Except for the exemplary nucleoporin dataset which is publicly available on the BioImage Archive (https://www.ebi.ac.uk/biostudies/files/S-BIAD8/Library/GFP/AB/raw/GFP_AB-AF647_190528_8.zip), ground-truth generated data and experimentally-obtained data used for testing and validating the neural network are available as supplementary data.

Code availability

Ground truth ROI simulating code, neural network training, validation code, classification code, ROI picker, GUI for simulating, training and validating DeepSense as well as pre-trained networks are all released under the MIT License on www.github.com/jdaniel/DeepSense. The dSTORM dataset processing code is released under the MIT License on www.github.com/jdaniel/StormProcessor.

Acknowledgements

JSJD is partially funded by a College Research Associateship (King's College, Cambridge). KC acknowledges the Elite programme for Postdocs of the Baden-Wurtemberg Stiftung for financial support. MMM is funded by a Junior Research Fellowship (King's College, Cambridge), DK is funded by an ERC advanced grant (669237). AJGS and RS are funded by an ERC consolidator grant (APOSITE).

Author contributions

JSJD conceived the project, RS performed the experiments, JSJD, MMM and FM developed the computational pipeline, RS, KC and JSJD tested and validated the code, DK and AJGS provided experimental infrastructure and JSJD wrote manuscript with input from all authors.

Competing interests

The authors declare no competing interests.

References

1. Das, S. K., Darshi, M., Cheley, S., Wallace, M. I. & Bayley, H. Membrane Protein Stoichiometry Determined from the Step-Wise Photobleaching of Dye-Labelled Subunits. *ChemBioChem* **8**, 994–999 (2007).
2. Ulbrich, M. H. & Isacoff, E. Y. Subunit counting in membrane-bound proteins. *Nat. Methods* **4**, 319–321 (2007).
3. Ha, T. Single-Molecule Fluorescence Resonance Energy Transfer. *Methods* **25**, 78–86 (2001).
4. Kapanidis, A. N. *et al.* Alternating-Laser Excitation of Single Molecules. *Acc. Chem. Res.* **38**, 523–533 (2005).
5. Heilemann, M. *et al.* Subdiffraction-Resolution Fluorescence Imaging with Conventional Fluorescent Probes. *Angew. Chem. Int. Ed.* **47**, 6172–6176 (2008).
6. Jungmann, R. *et al.* Single-Molecule Kinetics and Super-Resolution Microscopy by Fluorescence Imaging of Transient Binding on DNA Origami. *Nano Lett.* **10**, 4756–4761 (2010).
7. Hess, S. T., Girirajan, T. P. K. & Mason, M. D. Ultra-High Resolution Imaging by Fluorescence Photoactivation Localization Microscopy. *Biophys. J.* **91**, 4258–4272 (2006).
8. Betzig, E. *et al.* Imaging Intracellular Fluorescent Proteins at Nanometer Resolution. *Science* **313**, 1642–1645 (2006).
9. Rust, M. J., Bates, M. & Zhuang, X. Sub-diffraction-limit imaging by stochastic optical reconstruction microscopy (STORM). *Nat. Methods* **3**, 793–796 (2006).
10. Lowe, A. R. *et al.* Selectivity Mechanism of the Nuclear Pore Complex Characterized by Single Cargo Tracking. *Nature* **467**, 600–603 (2010).
11. Dahan, M. *et al.* Diffusion Dynamics of Glycine Receptors Revealed by Single-Quantum Dot Tracking. *Science* **302**, 442–445 (2003).
12. Yildiz, A. *et al.* Myosin V walks hand-over-hand: single fluorophore imaging with 1.5-nm localization. *Science* **300**, 2061–2065 (2003).

13. Izeddin, I. *et al.* Wavelet analysis for single molecule localization microscopy. *Opt. Express* **20**, 2081–2095 (2012).
14. Nehme, E., Weiss, L. E., Michaeli, T. & Shechtman, Y. Deep-STORM: super-resolution single-molecule microscopy by deep learning. *Optica* **5**, 458–464 (2018).
15. Nehme, E. *et al.* DeepSTORM3D: dense 3D localization microscopy and PSF design by deep learning. *Nat. Methods* **17**, 734–740 (2020).
16. Hirsch, M., Wareham, R. J., Martin-Fernandez, M. L., Hobson, M. P. & Rolfe, D. J. A Stochastic Model for Electron Multiplication Charge-Coupled Devices – From Theory to Practice. *PLOS ONE* **8**, e53671 (2013).
17. Thevathasan, J. V. *et al.* Nuclear pores as versatile reference standards for quantitative superresolution microscopy. *Nat. Methods* **16**, 1045–1053 (2019).
18. Möckl, L., Roy, A. R., Petrov, P. N. & Moerner, W. E. Accurate and rapid background estimation in single-molecule localization microscopy using the deep neural network BGnet. *Proc. Natl. Acad. Sci.* **117**, 60–67 (2020).
19. Xu, J. *et al.* Automated Stoichiometry Analysis of Single-Molecule Fluorescence Imaging Traces via Deep Learning. *J. Am. Chem. Soc.* **141**, 6976–6985 (2019).

Figures

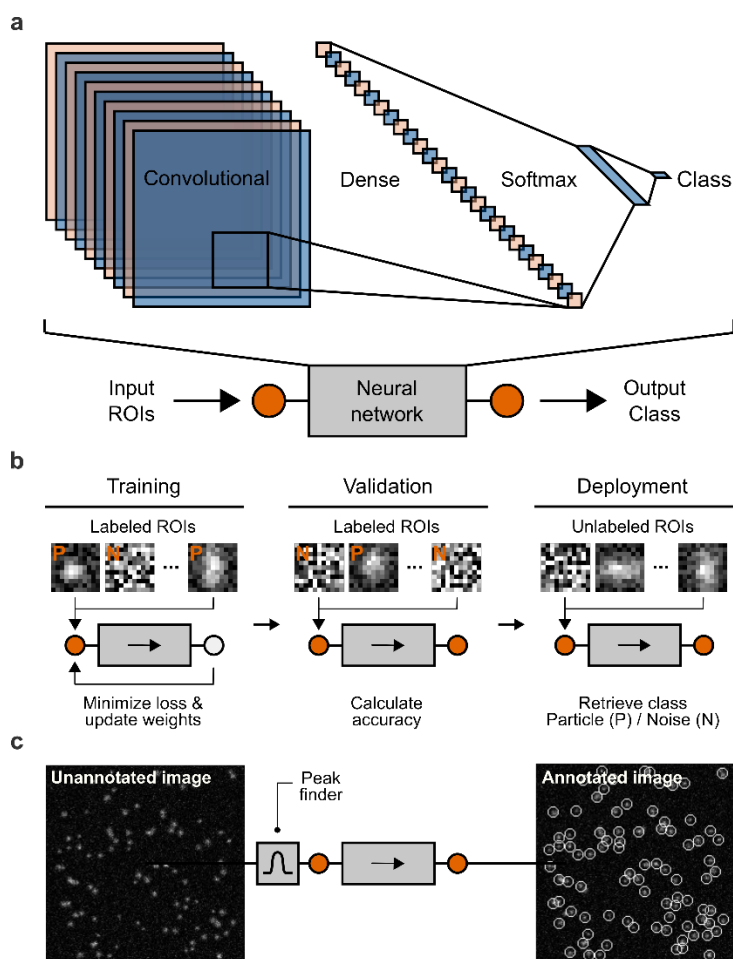


Figure 1 Single molecule segmentation pipeline using DeepSense. **(a)** Architecture of the neural network used in segmenting single molecule bursts from noise. The CNN layer is connected to a dense (i.e. fully-connected) layer. The dense layer is connected to a SoftMax for normalization which, in turn, is connected to a classification layer. Number of trainable parameters is 21,802. **(b)** The neural network is first GPU-trained on ground-truth, pre-labelled (i.e. annotated) ROIs divided into two classes; particle (P) or Noise (N). The ROIs are fed-forward into the network and a loss function is evaluated every mini-batch of 10 ROIs. Following training on a complete dataset, the network is validated on unseen data and the classification accuracy is calculated based on the correspondence between the generated and network-output classes. The network is finally tested on the CPU or GPU on unlabelled ROIs and the class for each ROI is extracted. **(c)** The network is, finally, deployed by feeding an image into a peak-finding algorithm which identifies regional maxima based on their 8 nearest neighbours' connectivity. The algorithm locates several hundred ROIs containing noise and particles and the ROIs are fed into the neural network which eventually segments the particles producing an annotated image.

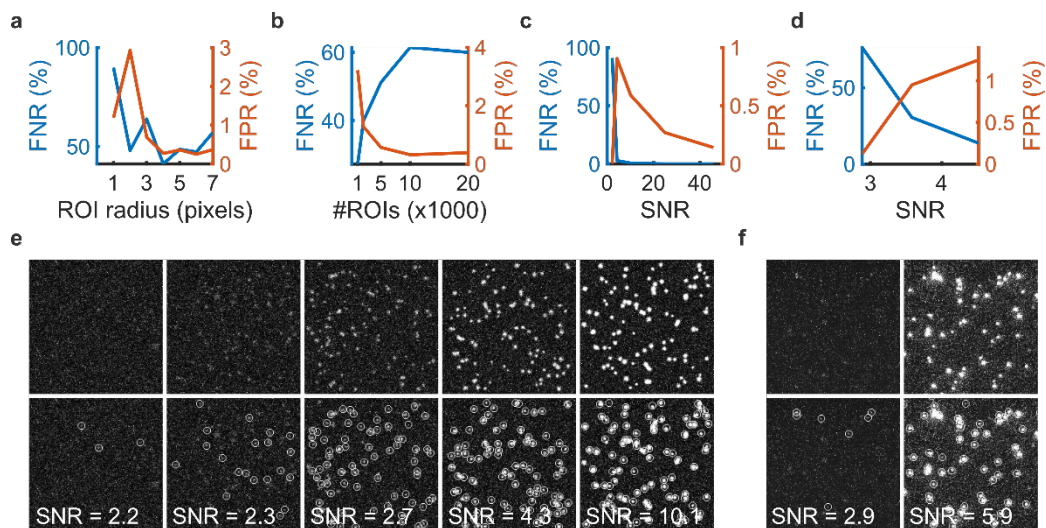


Figure 2 Systematic analysis of the performance of the neural network for parameter-tuning and validation purposes. Measurement of the FNR and FPR against **(a)** the radius of ROIs and **(b)** number of ROIs. **(c)** SNR of simulated ROIs and **(d)** SNR of experimentally-obtained ROIs. Exemplary **(e)** simulated and **(f)** experimentally-obtained images of particles at different SNRs.

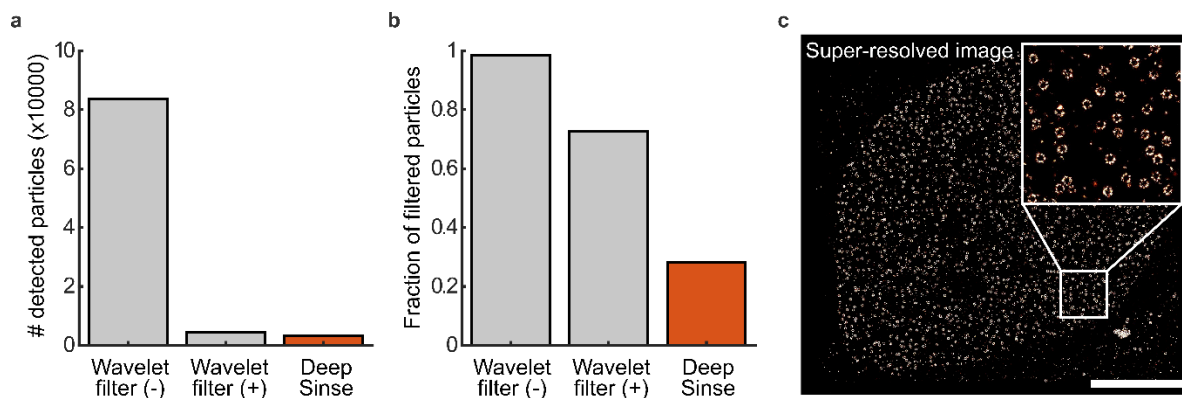


Figure 3 Comparison of the performance of a wavelet filter with DeepSinsse for blinking particles obtained from a publicly available exemplary dataset (see **Data availability**). **(a)** Number of detected particles and **(b)** fraction of rejected particles obtained using a wavelet filter and peak intensity threshold set to 0 photons [Wavelet filter (-)], wavelet filter and peak intensity threshold set to standard deviation of the first wavelet level [Wavelet filter (+)] and DeepSinsse for 1000 frames of the entire data set. **(c)** Super-resolved image of the exemplary data set produced following detection of particles using DeepSinsse and subsequent filtering.